Electron Confinement Effects in the EPR Spectra of Colloidal n-Type ZnO Quantum Dots

ARTICLE *in* THE JOURNAL OF PHYSICAL CHEMISTRY C · SEPTEMBER 2008

Impact Factor: 4.77 · DOI: 10.1021/jp804763y

4 AUTHORS, INCLUDING:

Stefan Thomas Ochsenbein
Empa - Swiss Federal Laboratories for Mat…
49 PUBLICATIONS **1,310** CITATIONS
SEE PROFILE

Victor Z. Polinger
University of Washington Seattle
63 PUBLICATIONS **696** CITATIONS
SEE PROFILE

Electron Confinement Effects in the EPR Spectra of Colloidal n-Type ZnO Quantum Dots

Kelly M. Whitaker, Stefan T. Ochsenbein, Victor Z. Polinger, and Daniel R. Gamelin*

Department of Chemistry and Center for Nanotechnology, University of Washington, Seattle, Washington 98195

Received: May 29, 2008

Additional unpaired electrons have been introduced into colloidal ZnO quantum dots (QDs) photochemically and investigated by experimental and theoretical methods to test various possible descriptions of their wave functions. For n-type ZnO QDs with diameters between 3.0 and 7.0 nm, electron paramagnetic resonance (EPR) spectroscopy reveals size-dependent g^* values in the range $1.960 < g^* < 1.968$ that are temperature independent and that rule out highly localized wave function descriptions. The size dependence of g^* is described well using a $\mathbf{k}\cdot\mathbf{p}$ perturbation expression, indicating similarity between these quantum confined electrons and free carriers in bulk ZnO. Model calculations confirm that significant electron density can reside on the QD surfaces only for surface well depths that can be experimentally excluded. Together, these results allow a firm experimental description of the photogenerated electrons as delocalized within the conduction bands of the colloidal ZnO QDs, making them excellent candidates for investigation of spin effects in semiconductor nanostructures.

I. Introduction

Electrons confined in semiconductor quantum dots (QDs) have been suggested as potential active components in quantum computation schemes based on spin qubits.[1] Several groups have studied the properties of confined electron spins in QDs grown epitaxially by molecular-beam epitaxy (MBE),[1−5] but the analogous properties of spins in colloidal QDs have received almost no attention. Transient Faraday rotation measurements following excitonic excitation have been used to probe both spin dynamics and electron g^* values in excitonic excited states of colloidal II−VI QDs.[6,7] Although several examples of II−VI or IV−VI colloidal QDs containing extra charge carriers in their ground states have been reported,[8−18] very few papers have addressed the spin properties of the resident carriers in this motif.[8,16,17] Previously published work shows that when additional electrons are photochemically injected into colloidal ZnO QDs, a strong $g^* \approx 1.96$ electron paramagnetic resonance (EPR) signal is observed.[16,17] Analysis of these spectra, particularly as a function of ^{67}Zn content in the QDs, demonstrated room-temperature electron spin dephasing dynamics on the nanosecond time scale that are largely governed by electron−nuclear hyperfine coupling with ^{67}Zn ($I = 5/2$) nuclei.[17] These data were analyzed assuming conduction-band-like (CB-like) electron probability distributions. In another study, inclusion of magnetic dopants within the charged colloidal ZnO QDs was also shown to strongly influence the electron's EPR spectrum.[16] For Co^{2+}-doped ZnO QDs, $e^- - Co^{2+}$ exchange interactions led to fast relaxation of the $g^* \approx 1.96$ EPR signal, even for QDs containing only one Co^{2+} ion. For Mn^{2+}-doped ZnO QDs, $e^- - Mn^{2+}$ exchange interactions led to broadening of the Mn^{2+} hyperfine structure that could be related to s−d magnetic exchange coupling interactions. Neither of these previous magnetic resonance studies directly investigated the influence of quantum confinement on the $g \approx 1.96$ EPR signal, however, and the electron's wave function was not well defined experimentally. As emphasized in a recent review,[18] it has generally not been possible to unequivocally determine whether ZnO nanocrystal charging indeed yields delocalized CB-like electrons rather than surface-trapped electrons, in part because interpretation of the poorly resolved optical changes that accompany charging remains contentious.[14,19]

In this paper, we describe the use of EPR spectroscopy to probe the influence of quantum confinement on the extra electrons in colloidal free-standing n-type ZnO QDs. Size effects have previously been observed in the EPR spectra of nanocrystalline ZnO powders with added donor impurities (Li^+ or Na^+),[20−23] but similar shallow donor EPR signals have also been observed in nanocrystalline ZnO powders without added donors,[24,25] indicating that native interfacial grain-boundary defects complicate the electronic properties of such powders. Indeed, interfacial donor defects are known to dominate the conductivities of ZnO powders.[26,27] The experiments described herein avoid such complications and allow the electrons of truly isolated colloidal n-type ZnO QDs to be probed by EPR spectroscopy. A clear size dependence of the resonance frequency is observed at both 300 and 20 K, and analysis allows the conclusion that these extra electrons are indeed delocalized throughout the ZnO nanocrystals, behaving as CB-like charge carriers. These colloidal n-type ZnO nanocrystals are thus excellent candidates for investigating the spin properties of quantum confined band-like charge carriers in freestanding semiconductor nanocrystals.

II. Experimental Section

Synthesis of the colloidal TOPO-capped ZnO QDs used here, their photochemical reduction, and their characterization by EPR spectroscopy were all performed using the methods previously described.[16,17,28] In short, an ethanolic solution of tetramethylammonium hydroxide was added dropwise into a solution of zinc acetate dissolved in dimethylsulfoxide. The resulting ZnO nanoparticles were washed, capped with trioctylphosphine oxide (TOPO), and resuspended in toluene. Particle diameters were estimated from the electronic absorption spectra and empirically established relationships between the band gap energies (E_g) and QD diameters,[29] from X-ray diffraction line broadening analyzed using the Scherrer equation, and from TEM measure-

* Corresponding author e-mail: gamelin@chem.washington.edu.

10.1021/jp804763y CCC: $40.75
Published on Web 08/23/2008

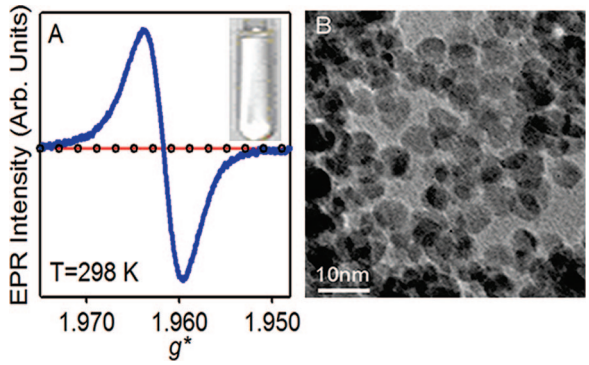

Figure 1. (A) 298 K EPR spectra of as-prepared (thin red line), photochemically reduced (thick blue line), and reoxidized (circles) colloidal $d = 7.0 \pm 1.7$ nm ZnO QDs suspended in toluene and photograph of as-prepared colloidal ZnO QDs (inset). (B) TEM image of as-prepared $d = 7.0 \pm 1.7$ nm ZnO QDs.

ments performed at Pacific Northwest National Laboratories using a JEOL 2010 transmission electron microscope (200 kV) with a high-brightness LaB6 filament as an electron source.

For charging experiments, the colloidal QDs were suspended in 98:2 toluene/ethanol (by volume), deaerated, and anaerobically sealed in quartz EPR tubes. All colloidal suspensions were dilute and of high optical quality, as illustrated in the inset of Figure 1A. These colloidal samples were exposed to UV irradiation from a BeamLok 2060 Ar^+ ion laser (Spectra Physics) or from an Hg arc lamp. UV excitation generates transient surface-trapped holes that can react with the added ethanol.[9] An unreacted electron is left behind that can then be probed spectroscopically using both magnetic resonance and optical techniques. The added electron is rapidly quenched upon exposure to air.

X-band (9.34 GHz) EPR spectra were collected on a Bruker EMX EPR spectrometer with samples held at room temperature or cooled down to 20 K using a Janis He flow cryostat. All EPR experiments described here were performed on anaerobic samples. Under these conditions, the EPR signal due to the added electron is kinetically stable and remains unchanged almost indefinitely. Kinetics measurements indicate a very slow electron decay constant of ~0.01/week at room temperature.[16,17] As previously suggested,[14,17] it is possible that multiple electrons may be introduced per QD. The EPR data presented here were all collected in the limit of low charging, where QDs possess at most one additional electron.

III. Results and Analysis

Figure 1A shows EPR spectra of as-prepared, photochemically reduced (n-type), and reoxidized colloidal ZnO QDs in toluene. Prior to photochemical reduction, no EPR signal is observed. Following photochemical reduction, an intense signal at $g^* \approx 1.96$ is observed that appears concomitantly with bleaching at the ZnO band gap absorption edge and with the appearance of a new near-IR absorption band as previously described.[16,17] After reoxidation, the EPR signal disappears and the electronic absorption spectrum quantitatively returns to its original intensities, indicating that the particles are not chemically altered over the course of the experiment. These optical changes agree well with previous results and have been proposed to result from ZnO CB filling.[9,10,12,14,16,17,30] The EPR signal in Figure 1A also behaves in precisely the same way as those previously reported for related samples.[16,17] The observed EPR signal thus represents a transition between $M_S = \pm 1/2$ substates of the $S = 1/2$ electron ground state, whose degeneracy is lifted

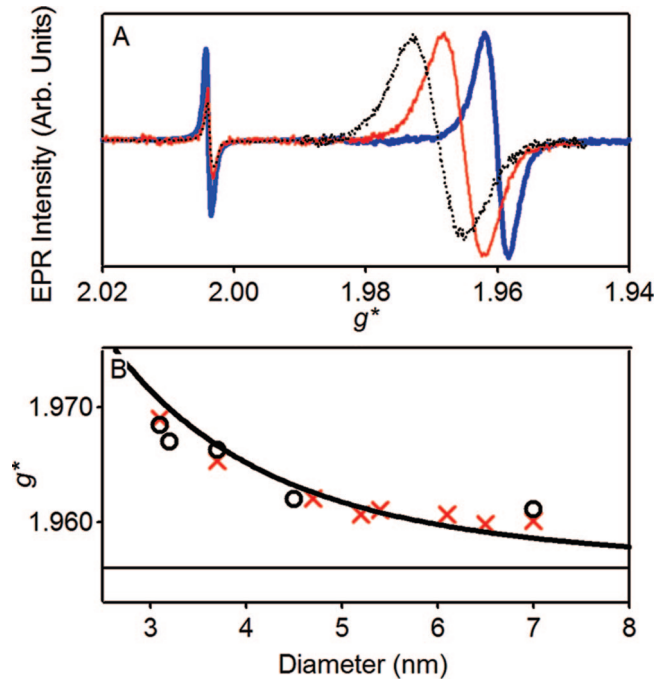

Figure 2. Dependence of the EPR signals observed for colloidal n-type ZnO QDs on the QD diameter. (A) 298 K EPR spectra of $d = 3.1$ nm (dotted black line), 3.7 nm (solid red line), and 7 nm (thick solid blue line) colloidal n-type ZnO QDs. (B) 298 K (red crosses) and 20 K (open circles) EPR g^* values plotted versus QD diameter. Fitting the 298 K data using eq 1 with P^2 fixed at 20 eV yielded $\Delta_{SO} = 40.3 \pm 0.4$ meV (thick solid line). The thin solid line at $g^* = 1.956$ is the value reported for shallow donors in bulk ZnO.[36,37]

by the applied magnetic field. Figure 1B shows a TEM image of representative ZnO QDs used in this study after they have been precipitated onto the TEM grid.

The EPR data in Figure 1 alone do not allow the nature of the electron's wave function in these photochemically reduced ZnO QDs to be deduced experimentally. Three limiting descriptions can be proposed: (i) the electrons are localized at defect sites (deep traps), (ii) the electrons are delocalized within the internal volumes of the ZnO QDs as CB-like electrons (quantized states or very shallow traps), or (iii) the electrons are delocalized over the surfaces of the QDs.[31]

To test the sensitivity of the added electrons to nanocrystal diameter, samples of various diameters were synthesized and charged, and their EPR spectra recorded. Figure 2A shows room temperature EPR spectra of ZnO QDs with three different diameters. The signal at $g = 2.0037$ is due to the diphenylpicrylhydrazyl radical (dpph), used as a reference signal for accurate determination of the ZnO g^* values. These data show a clear shift toward smaller g^* values with larger nanocrystal diameters. The added electron is thus sensitive to particle size. Figure 2B shows the g^* values from the spectra in Figure 2A plotted against particle diameter, along with data from several other colloidal ZnO QDs of different sizes that were charged and measured in the same fashion. Data collected at both room temperature and at 20 K are presented. A smooth increase in g^* with decreasing nanocrystal diameter is observed. The EPR signals for these freestanding colloidal ZnO QDs are in remarkable agreement with those reported for nanocrystalline powders of various different grain sizes, where they were described as arising from shallow donors.[20−25] Importantly, all of the g^* values in Figure 2 are significantly smaller than that of the free electron ($g_e = 2.0023$). As in bulk ZnO, the difference

between these resonances and that of the free electron is attributable to spin−orbit coupling.

The effect of spin−orbit coupling on g^* for CB-like electrons delocalized within ZnO QDs of various diameters can be described within the $\mathbf{k}\cdot\mathbf{p}$ band structure model in terms of band gap energies (E_g), valence-band spin−orbit coupling (Δ_{SO}), and interband mixing coefficients (P^2), as shown in the perturbation expression of eq 1.[25,32,33] An analytical expression relating the dependence of E_g on nanocrystal diameter has been provided by Brus.[34] For simplicity, both P^2 and Δ_{SO} are assumed to be independent of nanocrystal size. P^2 is approximately 20 eV for several II−VI and III−V semiconductors,[32] and $P^2 = 20$ eV has been used in other studies on ZnO.[24] The data in Figure 2B were thus fit using eq 1 by fixing $P^2 = 20$ eV and floating Δ_{SO}. A Δ_{SO} fit parameter of 40.3 ± 0.4 meV reproduces the data in Figure 2B reasonably well. This value is larger than and has the opposite sign from the literature value of $\Delta_{SO} = -3.5$ meV.[35] Equation 1 has been derived for cubic structures, however, where Δ_{SO} corresponds to the splitting between the top of the valence band and the so-called spin split-off band. The fit value for Δ_{SO}, in fact, agrees very well with the total splitting (~40 meV) between the top of the valence band and the third highest band in this wurtzite lattice, a splitting that reflects the combined contributions from spin−orbit coupling and the crystal-field splitting. Additionally, when $\Delta_{SO} = 40.3$ meV, the $\mathbf{k}\cdot\mathbf{p}$ calculated curve extrapolates to the bulk ZnO shallow donor value of $g^* = 1.956$,[36,37] represented by the solid line in Figure 2B, indicating that these same parameters also describe CB-like electrons in bulk ZnO. The minor discrepancy between experimental and calculated curves in Figure 2B may arise from the contributions of nanocrystal shape anisotropy[38] or from surface effects[33] (vide infra). Nevertheless, eq 1 reproduces the experimental results well in both sign and magnitude of the shift in g^* with QD diameter using parameters for P^2 and Δ_{SO} that are both reasonable and consistent with previous literature results.

$$g^* = g_e - \frac{2}{3}\left(\frac{P^2\Delta_{SO}}{E_g(E_g + \Delta_{SO})}\right) \quad (1)$$

The agreement between the calculated curve from eq 1 and the diameter dependence of the 300 K EPR signals shown in Figure 2 indicates that these electrons are not deeply trapped. A deeply trapped electron would have a g^* value that is independent of particle diameter and likely substantially closer to that of the free electron ($g_e = 2.0023$). At most, the electrons observed here may be associated with shallow traps whose energies are also shifted with particle size as the CB edge moves due to quantum confinement.[34] EPR spectra were, therefore, measured at cryogenic temperatures in efforts to freeze out the electrons in such traps. As shown in Figure 2B, almost identical g^* values are observed at 20 and 300 K for all nanocrystal diameters. If the injected electrons localize at cryogenic temperatures, then g^* should be significantly different at 20 K ($kT = 1.7$ meV) than at room temperature. These data therefore provide strong evidence indicating that the electron wave function is highly delocalized throughout this entire temperature range. A delocalized electron description is consistent with the large oscillator strength of the associated IR absorption band previously described and attributed to intra-CB excitation.[9,12,14,16,17,30] A delocalized electron is also consistent with assignment[39,40] of the green visible photoluminescence of such ZnO QDs to the recombination of a shallowly trapped electron and a deeply trapped hole; evidence that this electron is CB-like in the green emitting excited state can be seen from the size dependence of the visible photoluminescence energy, which follows the size dependence anticipated from the electron effective mass in ZnO.[40] Finally, similar EPR spectra have previously been associated with shallow electron donor levels residing ~0.1 eV below the CB edge in ZnO nanocrystalline powders,[20−25] and even shallower in bulk ZnO.[41] Although these literature results relate only indirectly to the present case of stable electrons in colloidal ZnO QDs, they do suggest that the electrons probed in these freestanding QDs by EPR spectroscopy are similar to those probed by other techniques and in other related forms of ZnO. On the basis of the data in Figure 2, scenario (i) can thus be eliminated. The added electrons do not localize on the ZnO QD surfaces or in any other traps.

Discerning between a delocalized surface electron and a delocalized CB electron is more challenging. Delocalized surface states originating from dangling bonds often occur in the gap for bulk and thin-film semiconductors.[31] In QDs, such surface states might gain importance due to the large surface-to-volume ratios. The EPR data for these colloidal ZnO QDs are similar to those attributed to shallow donor defects in nanocrystalline powders.[20−25] EPR signals arising from collections of defects along grain boundaries could be analogous to the ones anticipated from scenario (iii) in the freestanding ZnO QDs. Finally, upon quenching of the hole from the excitonic states of these QDs, the absence of the stabilizing electron−hole interaction might cause the remaining electron to move toward the nanocrystal surfaces for charge compensation. These considerations suggest that delocalized surface states (scenario iii) cannot be ruled out *a priori*.

To explore the possibility of a delocalized surface state, radial probability distribution functions of electrons in idealized spherical nanostructures were calculated (see Supporting Information for details). Parameters were chosen to represent QDs with total diameters of $d = 5.0$ nm that include a lower-potential surface layer of thickness $a = 0.5$ nm, corresponding to approximately one ZnO monolayer. The CB potential (U_1) associated with the core of the sphere is assumed to be higher than the surface well potential (fixed at zero), and an outer surface potential (U_2) is held at 5 eV above U_1, a value that corresponds to the electron affinity of ZnO.[42] The noninfinite outer potential allows electron tunneling beyond the crystal outer surface, an important consideration for surface states. U_1 is thus effectively the depth of the surface potential well. Figure 3A illustrates the parameters used. Within this approach, eq 2 gives the analytical condition that must be met to have at least one localized solution in the surface potential well. Equation 2 is written in atomic units, where $\hbar = 1$, $e = 1$, and Bohr radius $a_B = 1$. Because the electron's effective mass for such a surface state is unknown, the real mass of an electron ($m_e^* = 1.0\ m_0$) was used rather than the reduced effective mass of the electron in ZnO ($m_e^* \approx 0.26\ m_0$[35,43]) in order to maximize the probability of surface state formation for illustration purposes. The true m_e^* for the surface state is undoubtedly smaller than $1.0\ m_0$, and these calculations therefore represent lower limits for the surface well depths that would be required to form surface states.

$$a\sqrt{2U_1} + \arcsin\left(\sqrt{\frac{U_1}{U_2}}\right) \geq \frac{\pi}{2} \quad (2)$$

When the inequality of eq 2 is solved numerically for a QD with $R = 2.5$ nm, $a = 0.5$ nm, and $U_2 = U_1 + 5$ eV, it yields the result that U_1 must be greater than 0.27 eV to generate a wave function having the maximum in its volume-weighted probability distribution function ($\Psi^2 r^2$) within the surface

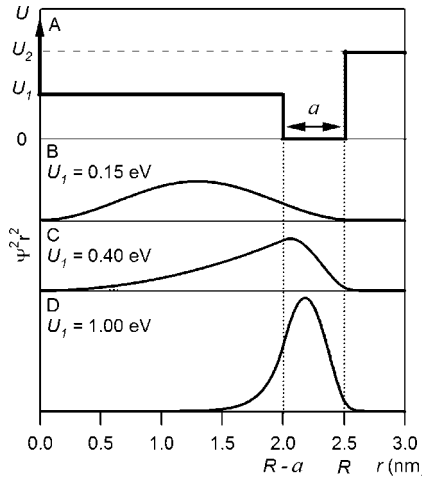

Figure 3. (A) Schematic illustration of the parameters used to calculate electron wave functions in n-type ZnO nanocrystals. U_1 = potential offset between core and surface well, a = surface well width, U_2 = (U_1 + 5 eV). Electron radial probability distributions (Ψ^2r^2) calculated for (B) U_1 = 0.15 eV, (C) U_1 = 0.40 eV, and (D) U_1 = 1.00 eV, all with a = 0.5 nm, R = 2.5 nm, and m_e^* = 1.0 m_0.

potential well. If this condition is not met (U_1 < 0.27 eV), then Ψ^2r^2 has its maximum within the inner volume of the sphere.

For more detailed insight into the role of surface well depth, the electronic wave functions calculated for three specific surface−well depths (0.15, 0.40, and 1.00 eV) are presented in Figure 3, panels B−D, plotted as Ψ^2r^2 versus r. Figure 3B shows the electronic wave function calculated for U_1 = 0.15 eV. This well depth is considered to be most consistent with the electron trap depths estimated from the photoluminescence and EPR results for the related samples discussed above.[20−25,39−41] For this well depth, the electron remains delocalized throughout the nanocrystal and is only slightly perturbed by the presence of the surface well (Figure 3B), even in the extreme scenario of m_e^* = 1.0 m_0.

To illustrate the conditions that would be required to shift significant electron density out to the ZnO QD surfaces, panels C and D of Figure 3 depict the wave functions calculated for U_1 = 0.40 and 1.00 eV, respectively. Both of these well depths are significantly greater than estimates provided by experimental data. The former is shown because it is close to the shallowest well depth at which the Ψ^2r^2 maximum shifts into the surface layer (U_1 = 0.27 eV). Even in this scenario, only ∼30% of the total electron density resides in the surface layer. The case of U_1 = 1.00 eV shown in Figure 3D is included to illustrate the conditions required to shift a major fraction of electron density out to the surface. In this case, ∼80% of the electron density resides in the surface layer for m_e^* = 1.0 m_0. This value of U_1 = 1.0 eV is inconsistent not only with PL data but also with the chemical reducing power of the extra electrons found in reactions with oxidizable substrates,[9,17] and it is included here only for illustrative purposes. Reduction of the electron effective mass to more realistic values only shifts electron probability density away from the nanocrystal surfaces. Overall, these calculations argue strongly against the possibility that the photochemically generated electrons observed in Figures 1 and 2 have significant surface character, and scenario (iii) can be ruled out. Scenario (ii) is, thus, most consistent with experiment, and the extra electrons are concluded to be truly CB-like within these ZnO QDs.

IV. Conclusions

The 300 and 20 K EPR data reported here indicate that photochemical reduction of colloidal ZnO QDs generates delocalized CB-like electrons. The diameter dependence of the EPR resonance frequency is reproduced well by a simple **k·p** band model. The possibility of deep electron trapping is eliminated directly by the experimental diameter dependence of g^* and its large deviation from g_e = 2.0023. Shallower electron trapping is also not observed down to cryogenic temperatures. Wave function calculations indicate that even delocalized surface states are unfavorable for such charged QDs. These findings agree very well with previous wave function descriptions from idealized tight-binding calculations,[30] with magnetic resonance results for related but more complicated nanocrystalline ZnO powders,[20−25] and with recent TRFR data probing electron spin dynamics in these colloidal ZnO nanocrystals.[44]

In the broader context, these colloidal n-type ZnO QDs appear to be unique among colloidal II−VI, III−V, or IV−VI QDs in that they allow CB electrons to be kinetically stabilized and their physical characteristics directly probed by conventional magnetic resonance techniques. With the conclusion that the extra electrons are truly quantum confined, possessing delocalized CB-like wave functions, this motif of colloidal n-type ZnO QDs becomes increasingly attractive as the model system for studying charge carrier spins, spin dynamics, carrier-dopant magnetic exchange interactions, and other carrier-dependent phenomena in truly freestanding semiconductor nanostructures.

Acknowledgment. This work was funded by the NSF ((CRC-0628252) to D.R.G. and DGE-0504573 (IGERT fellowship) to K.M.W.), the Research Corporation, the Dreyfus Foundation, and the Sloan Foundation. Postdoctoral fellowship support from the Swiss National Science Foundation (to S.T.O.) is gratefully acknowledged. The authors thank Dr. Chongmin Wang for assistance with TEM measurements, Vladimir Vlaskin, Alyssa Smith Begg, Dr. Rémi Beaulac, and Professor Bruce Robinson for valuable input and assistance. Instrumentation support from the Center for Ecogenetics and Environmental Health UW center grant No. P30 ES07033 from the National Institutes of Environmental Health Sciences, NIH, is gratefully acknowledged.

Supporting Information Available: Details of the wave function calculations are available free of charge via the Internet at http://pubs.acs.org.

References and Notes

(1) Cerletti, V.; Coish, W. A.; Gywat, O.; Loss, D. *Nanotechnology* **2005**, *16*, R27-R49.
(2) Kouwenhoven, L. P.; Austing, D. G.; Tarucha, S. *Rep. Prog. Phys.* **2001**, *64*, 701–736.
(3) Hanson, R.; Witkamp, B.; Vandersypen, L. M. K.; Willems van Beveren, L. H.; Elzerman, J. M.; Kouwenhoven, L. P. *Phys. Rev. Lett.* **2003**, *91*, 196802.
(4) Braun, P.-F.; Marie, X.; Lombez, L.; Urbaszek, B.; Amand, T.; Renucci, P.; Kalevich, V. K.; Kavokin, K. V.; Krebs, O.; Voisin, P.; Matsumoto, Y. *Phys. Rev. Lett.* **2005**, *94*, 116601.
(5) Petta, J. R.; Johnson, A. C.; Taylor, J. M.; Laird, E. A.; Yacoby, A.; Lukin, M. D.; Markus, C. M.; Hanson, M. P.; Gossard, A. C. *Science* **2005**, *309*, 2180–2184.
(6) Gupta, J. A.; Awschalom, D. D.; Peng, X.; Alivisatos, A. P. *Phys. Rev. B* **1999**, *59*, R10421–R10424.
(7) Gupta, J. A.; Awschalom, D. D.; Efros, Al. L.; Rodina, A. V. *Phys. Rev. B* **2002**, *66*, 125307.
(8) Stern, N. P.; Poggio, M.; Bartl, M. H.; Hu, E. L.; Stucky, G. D.; Awschalom, D. D. *Phys. Rev. B* **2005**, *72*, 161303(R).
(9) Haase, M.; Weller, H.; Henglein, A. *J. Phys. Chem.* **1988**, *92*, 482–487.
(10) Hoyer, P.; Weller, H. *Chem. Phys. Lett.* **1994**, *221*, 379–384.

(11) Shim, M.; Guyot-Sionnest, P. *Nature* **2000**, *407*, 981–983.
(12) Shim, M.; Guyot-Sionnest, P. *J. Am. Chem. Soc.* **2001**, *123*, 11651–11654.
(13) Shim, M.; Wang, C.; Guyot-Sionnest, P. *J. Phys. Chem. B* **2001**, *105*, 2369–2373.
(14) Germeau, A.; Roest, A. L.; Vanmaekelbergh, D.; Allan, G.; Delerue, C.; Meulenkamp, E. A. *Phys. Rev. Lett.* **2003**, *90*, 097401.
(15) Wehrenberg, B. L.; Guyot-Sionnest, P. *J. Am. Chem. Soc.* **2003**, *125*, 7806–7807.
(16) Liu, W. K.; Whitaker, K. M.; Kittilstved, K. R.; Gamelin, D. R. *J. Am. Chem. Soc.* **2006**, *128*, 3910–3911.
(17) Liu, W. K.; Whitaker, K. M.; Smith, A. L.; Kittilstved, K. R.; Robinson, B. H.; Gamelin, D. R. *Phys. Rev. Lett.* **2007**, *98*, 186804.
(18) Guyot-Sionnest, P. *Microchim. Acta* **2008**, *160*, 309–314.
(19) Shim, M.; Guyot-Sionnest, P. *Phys. Rev. Lett.* **2003**, *91*, 169703.
(20) Orlinskii, S. B.; Schmidt, J.; Baranov, P. G.; Hofmann, D. M.; de Mello Donegá, C.; Meijerink, A. *Phys. Rev. Lett.* **2004**, *92*, 047603.
(21) Orlinskii, S. B.; Schmidt, J.; Groenen, E. J. J.; Baranov, P. G.; de Mello Donegá, C.; Meijerink, A. *Phys. Rev. Lett.* **2005**, *94*, 097602.
(22) Orlinskii, S. B.; Blok, H.; Schmidt, J.; Baranov, P. G.; de Mello Donegá, C.; Meijerink, A. *Phys. Rev. B* **2006**, *74*, 045204.
(23) Orlinskii, S. B.; Schmidt, J.; Baranov, P. G.; Lorrmann, V.; Riedel, I.; Rauh, D.; Dyakonov, V. *Phys. Rev. B* **2008**, *77*, 115334.
(24) Zhou, H. Optical and Magnetic Resonance Properties of II−VI Quantum Dots. Ph.D. Thesis, Justus-Liebig University, 2002.
(25) Zhou, H.; Hofstaetter, A.; Hofmann, D. M.; Meyer, B. K. *Microelectron. Eng.* **2003**, *66*, 59–64.
(26) Lee, J.; Hwang, J.-H.; Mashek, J. J.; Mason, T. O.; Miller, A. E.; Siegel, R. W. *J. Mater. Res.* **1995**, *10*, 2295–2300.
(27) Jose, J.; Abdul Khadar, M. *Mat. Sci. Eng.* **2001**, *A304−306*, 810–813.
(28) Schwartz, D. A.; Norberg, N. S.; Nguyen, Q. P.; Parker, J. M.; Gamelin, D. R. *J. Am. Chem. Soc.* **2003**, *125*, 13205–13218.
(29) Meulenkamp, E. A. *J. Phys. Chem. B* **1998**, *102*, 5566–5572.
(30) Roest, A. L.; Germeau, A.; Kelly, J. J.; Vanmaekelbergh, D.; Allan, G.; Meulenkamp, E. A. *Chem. Phys. Chem.* **2003**, *4*, 959–966.
(31) Davison, S.; Steslicka, M., *Basic Theory of Surface States*; Oxford University Press: New York, 1992.
(32) Hermann, C.; Weisbuch, C. *Phys. Rev. B* **1977**, *15*, 823–833.
(33) Rodina, A. V.; Efros, Al. L.; Rosen, M.; Meyer, B. K. *Mater. Sci. Eng., C* **2002**, *19*, 435–438.
(34) Brus, L. *J. Phys. Chem.* **1986**, *90*, 2555–2560.
(35) Madelung, O., *Semiconductors: Data Handbook*, 3rd ed; Springer: Berlin, 2004.
(36) Carlos, W. E.; Glaser, E. R.; Look, D. C. *Physica B* **2001**, *308−310*, 976–979.
(37) Gonzalez, C.; Block, D.; Cox, R. T.; Hervé, A. *J. Cryst. Growth* **1982**, *59*, 357–362.
(38) Kuno, M.; Nirmal, M.; Bawendi, M. G.; Efros, A.; Rosen, M. *J. Chem. Phys.* **1998**, *108*, 4242–4247.
(39) van Dijken, A.; Meulenkamp, E. A.; Vanmaekelbergh, D.; Meijerink, A. *J. Phys. Chem. B* **2000**, *104*, 1715–1723.
(40) van Dijken, A.; Meulenkamp, E. A.; Vanmaekelbergh, D.; Meijerink, A. *J. Lumin.* **2000**, *90*, 123–128.
(41) Hofmann, D. M.; Hofstaetter, A.; Leiter, F.; Zhou, H.; Henecker, F.; Meyer, B. K.; Orlinskii, S. B.; Schmidt, J.; Baranov, P. G. *Phys. Rev. Lett.* **2002**, *88*, 045504.
(42) Brus, L. E. *J. Chem. Phys.* **1983**, *79*, 5566–5571.
(43) Meyer, B. K.; Alves, H.; Hofmann, D. M.; Kriegseis, W.; Forster, D.; Bertram, F.; Christen, J.; Hoffmann, A.; Straβburg, M.; Dworzak, M.; Haboeck, U.; Rodina, A. V. *Phys. Stat. Sol. B* **2004**, *241*, 231–260.
(44) Janssen, N.; Whitaker, K. M.; Gamelin, D. R.; Bratschitsch, R. *Nano Lett.* **2008**, *8*, 1991–1994.

JP804763Y